AD-A157 476 SCALING CALCULATIONS FOR A RELATIVISTIC GYROTRON(U) 1/1
NAVAL RESEARCH LAB WASHINGTON DC A W FLIFLET 31 JUL 85
NRL-MR-5598

UNCLASSIFIED F/G 9/1 NL

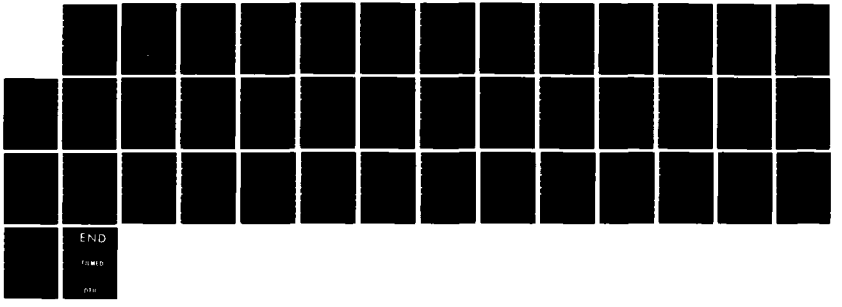

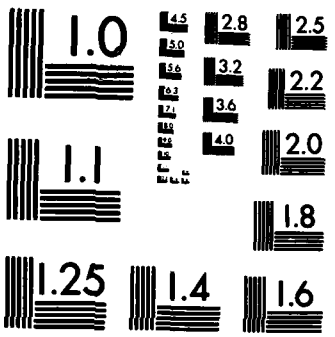

NRL Memorandum Report 5598

Scaling Calculations for a Relativistic Gyrotron

A. W. FLIFLET

High Power Electromagnetic Radiation Branch
Plasma Physics Division

July 31, 1985

This work was supported by the Defense Nuclear Agency under Subtask X99QMXVF, work unit 00007 and work unit title "Gyrotron Development," also by the Lawrence Livermore National Laboratory and the Office of Naval Research.

NAVAL RESEARCH LABORATORY
Washington, D.C.

SECURITY CLASSIFICATION OF THIS PAGE

REPORT DOCUMENTATION PAGE

1a REPORT SECURITY CLASSIFICATION UNCLASSIFIED	1b RESTRICTIVE MARKINGS
2a SECURITY CLASSIFICATION AUTHORITY	3 DISTRIBUTION / AVAILABILITY OF REPORT Approved for public release; distribution unlimited.
2b DECLASSIFICATION / DOWNGRADING SCHEDULE	
4 PERFORMING ORGANIZATION REPORT NUMBER(S) NRL Memorandum Report 5598	5 MONITORING ORGANIZATION REPORT NUMBER(S)
6a NAME OF PERFORMING ORGANIZATION Naval Research Laboratory 6b OFFICE SYMBOL (If applicable) Code 4740	7a NAME OF MONITORING ORGANIZATION
6c ADDRESS (City, State, and ZIP Code) Washington, DC 20375-5000	7b ADDRESS (City, State, and ZIP Code)
8a NAME OF FUNDING / SPONSORING ORGANIZATION DNA and ONR 8b OFFICE SYMBOL (If applicable)	9 PROCUREMENT INSTRUMENT IDENTIFICATION NUMBER
8c ADDRESS (City, State, and ZIP Code) Washington, DC 20305 Washington, DC 22217	10 SOURCE OF FUNDING NUMBERS PROGRAM ELEMENT NO: (See page ii) / PROJECT NO / TASK NO. / WORK UNIT ACCESSION NO.
11 TITLE (Include Security Classification) Scaling Calculations for a Relativistic Gyrotron	
12 PERSONAL AUTHOR(S) Fliflet, A.W.	
13a TYPE OF REPORT Interim 13b TIME COVERED FROM 3/84 TO 3/85	14 DATE OF REPORT (Year, Month, Day) 1985 July 31 15 PAGE COUNT 42
16 SUPPLEMENTARY NOTATION (See page ii)	

17 COSATI CODES			18 SUBJECT TERMS (Continue on reverse if necessary and identify by block number)
FIELD	GROUP	SUB-GROUP	Relativistic gyrotron; Millimeter wave radiation; High peak power generation

19 ABSTRACT (Continue on reverse if necessary and identify by block number)

The relativistic gyrotron is under development ~~at NRL~~ as an ultra-high power source of millimeter wave radiation. The purpose of the present study is to estimate the optimum operating characteristics of gyrotrons based on multi-kiloampere, mega-electron volt electron beams. Gyrotrons with weakly relativistic, moderate current electron beams have demonstrated very high efficiency and average power at millimeter wavelengths and the possibility of achieving good efficiencies at very high peak powers is of interest. Compared to other high power millimeter wave generators, gyrotrons are relatively insensitive to electron beam velocity spread and thus appear well suited to device configurations based on high current pulseline accelerators. The results of this study indicate that the relativistic gyrotron has potential for achieving high efficiency (15-30%) using relativistic electron beams with $\gamma \sim 2\text{-}3$. Optimum efficiency occurs for short interaction lengths; characterized by 4-8 cyclotron periods. Such short interaction lengths lead to the possibility of very high peak power generation using multi-kiloampere

(Continues)

20 DISTRIBUTION / AVAILABILITY OF ABSTRACT ☒ UNCLASSIFIED/UNLIMITED ☐ SAME AS RPT ☐ DTIC USERS	21 ABSTRACT SECURITY CLASSIFICATION UNCLASSIFIED
22a NAME OF RESPONSIBLE INDIVIDUAL Arne W. Fliflet	22b TELEPHONE (Include Area Code) (202) 767-2469 22c. OFFICE SYMBOL Code 4740

DD FORM 1473, 84 MAR 83 APR edition may be used until exhausted
All other editions are obsolete

SECURITY CLASSIFICATION OF THIS PAGE

10. SOURCE OF FUNDING NUMBERS

PROGRAM ELEMENT NO.	PROJECT NO.	TASK NO.	WORK UNIT ACCESSION NO.
62715H	~~84-687~~		DN480-686
61153N	RR011-09-41		DN880-061

16. SUPPLEMENTARY NOTATION

This work was supported by the Defense Nuclear Agency under Subtask X99QMXVF, work unit 00007 and work unit title "Gyrotron Development," also by the Lawrence Livermore National Laboratory and the Office of Naval Research.

19. ABSTRACT (Continued)

beams: 100-300 MW with a 600 keV beam and ~1 GW with a 1 MeV beam. The output power risetime has been estimated to be a few nanoseconds for a low Q oscillator at 35 GHz which implies the gyrotron interaction can be readily investigated using a 20-100 nsec pulseline accelerator.

CONTENTS

A-1

SCALING CALCULATIONS FOR A RELATIVISTIC GYROTRON

I. Introduction:

The gyrotron oscillator is under development as a source of high power millimeter-wave radiation. Research in the U. S. to date has emphasized high average power devices based on thermionic cathode technology. Output powers up to a megawatt have been achieved by such devices which are based on high quality moderate voltage ($\lesssim$ 100 keV) electron beams with currents of $\lesssim$ 50 Amps. High efficiencies $\sim$ 50% have beeen demonstrated. Future directed energy applications of high power millimeter-wave radiation may require sources with peak power in the gigawatt range. It is therefore of interest to investigate the peak power potential of a relativistic gyrotron with a mega-electronvolt, milti-kilomampere electron beam. Such an electron beam can be generated for short pulse lengths ($\lesssim$ 100 nsec) using a pulseline accelerator with a field emission (cold) cathode. An important objective of this work is to obtain design parameters for a cold cathode gyrotron experiment based on a 600 kV, 6kA, 55 nsec Febetron pulser. A second objective is to investigate scaling to higher voltage to increase output power.

Section 2 of this report describes scaling parameters and design constraints for a relativistic gyrotron. The results of calculations are given in Section 3. The non-linear, slow-time-scale equations of motion used for these calculations are derived in the Appendix.

Manuscript approved May 23, 1985.

II. Gyrotron Scaling Theory and Design Constraints

This section describes scaling parameters and constraints for a relativistic gyrotron with a megavolt, multi-kiloampere electron beam. The configuration analyzed corresponds to a cylindrical resonator and a thin annular electron beam with the beam radius chosen to coincide with a maximum of the resonator electric field.

The gyrotron is a particular case of the Cyclotron Resonance Maser (CRM). The resonance condition is

$$\omega - k_{\parallel} v_{\parallel} - s\Omega/\gamma \approx 0 \qquad (1)$$

where ω is the rf frequency, Ω is the non-relativistic cyclotron frequency, γ is the relativistic mass ratio, $v_{\parallel}$ is the axial electron velocity, $k_{\parallel}$ is the axial propagation number, and s is the harmonic number. In the gyrotron the electron beam interacts most effectively with a TE type mode which is close to cut-off in the resonator. Thus, the gyrotron corresponds to the case $k_{\parallel} v_{\parallel} << \omega \approx s\Omega/\gamma$. The present calculations consider only the fundamental harmonic interaction (s=1) as this yields the highest power and is least subject to mode competition.

The basic gyrotron interaction is characterized by five parameters: the e-beam relativistic factor γ , the e-beam pitch ratio $\alpha = v_{\perp}/v_{\parallel}$; the number of cyclotron orbits an electron makes traversing the resonator, N_c; the applied axial magnetic field, B_0; and the amplitude of the rf electric field at the e-beam position, E_b. Gyrotron designs for high power are subject to constraints on the minimum resonator Q, the maximum electric fields at the cavity wall, the space-charge limit on beam current and requirements for stability of single mode operation. To optimize the gyrotron design for a given e-beam energy, characterized by γ_o , and pitch ratio α , it is convenient to use the number of cyclotron orbits N_c as the scaling parameter. The applied magnetic field, B_0, and the electric field amplitude at the e-beam are then varied to optimize the efficiency.

In terms of N_c, the interaction length is given by

$$L = \frac{2\pi}{\omega_c} v_{\parallel o} N_c = (N_c + 1) \lambda \beta_{\parallel o} \tag{2}$$

where Eq. (5) below has been used and

$$\beta_{\parallel o} = \left[\frac{1 - 1/\gamma_o^2}{1 + \alpha^2} \right] \tag{3}$$

is the normalized axial velocity, ω_c is the relativistic cyclotron frequency ($\omega_c = \Omega/\gamma_o$), and $\lambda = \frac{c}{f}$ is the free-space wavelength. The rf fields in a cylindrical cavity can be expressed in terms of the axial profile function h(z). The profile function depends on several factors including the interaction itself; however, a reasonable approximation for scaling calculations is to assume a sinusoidal profile:

$$h(z) = \sin k_{\parallel} z \tag{4}$$

where $k_{\parallel} = \pi/L$. The interaction efficiency is optimized when the cyclotron frequency is detuned from the resonance frequency by approximately the interaction bandwidth, i.e.,

$$\omega - \omega_c \approx \frac{\omega_c}{N_c} \tag{5}$$

Thus a good estimate for the optimum magnetic field is given by

$$B_o = \frac{m}{|e|} \frac{\gamma_o \omega}{1 + 1/N_c} \tag{6}$$

which was used in these calculations. This leaves the electric field amplitude E_b as the only optimization parameter.

Estimates for the electronic efficiency were obtained by integrating a set of equations of motion for an electron in the cavity and averaging over the initial phase of the electron entering the cavity. A tractable set of non-linear equations based on a slow-time-scale formulation developed previously was used. For this application, the equations derived in reference 1 for a TE circular waveguide mode have been generalized to include the interaction with the rf magnetic field component, which is important at relativistic e-beam energies. A derivation of the equations of motion is given in the Appendix. Electron beam self-field effects and thermal effects are neglected.

As shown in the Appendix, the slow-time-scale equations of motion for a gyrotron interacting at the sth harmonic with a TE circular waveguide mode which is close to cutoff can be written in the form:

$$\frac{du_t}{d\zeta} = -\frac{1}{2}\frac{\gamma}{u_z}\left[J_{s-1}\left(\frac{u_t}{\bar{\Omega}_{zo}}\right) - J_{s+1}\left(\frac{u_t}{\bar{\Omega}_{zo}}\right)\right] \mathrm{Re}\left\{\bar{E}_s\left(h - \frac{iu_z}{\gamma\bar{\omega}}\frac{dh}{d\zeta}\right) e^{is\Lambda}\right\} + \frac{u_t}{2\bar{\Omega}_{zo}}\frac{d\bar{\Omega}_{zo}}{d\zeta} \quad (7a)$$

$$\frac{d\Lambda}{d\zeta} = -\frac{1}{2}\frac{\gamma}{u_z u_t}\left[J_{s-1}\left(\frac{u_t}{\bar{\Omega}_{zo}}\right) + J_{s+1}\left(\frac{u_t}{\bar{\Omega}_{zo}}\right)\right]$$

$$\mathrm{Re}\left\{\bar{E}_s\left[i\left(h - \frac{iu_z}{\gamma\bar{\omega}}\frac{dh}{d\zeta}\right) - \frac{u_t^2}{\gamma\bar{\omega}}\frac{h}{\bar{\Omega}_{zo}}\right] e^{is\Lambda}\right\} + \frac{\gamma}{u_z}\left(\frac{\bar{\omega}}{s} - \frac{\Omega_{zo}}{\gamma}\right) \quad (7b)$$

$$\frac{du_z}{d\zeta} = -\frac{1}{2}\frac{1}{\bar{\omega}}\frac{u_t}{u_z}\left[J_{s-1}\left(\frac{u_t}{\bar{\Omega}_{zo}}\right) - J_{s+1}\left(\frac{u_t}{\bar{\Omega}_{zo}}\right)\right] \mathrm{Re}\left\{\bar{E}_s\frac{dh}{d\zeta}e^{is\Lambda}\right\} - \frac{u_t}{u_z}\frac{1}{\bar{\Omega}_{zo}}\frac{d\bar{\Omega}_{zo}}{d\zeta} \quad (7c)$$

In Equations (7) u_t and Λ are slow-time-scale variables for the magnitude and phase of the transverse momentum, and u_z is the axial momentum. ζ is the axial coordinate and γ is the relativistic factor $(\gamma^2 = 1 + u_t^2 + u_z^2)$. E_s is the effective electric field at the beam and h is the normalized axial profile function of the electromagnetic mode $\{f = |f_{max}|\, h(z)\}$. J_{s-1} is a regular Bessel function.

$\bar{\omega}$ is the normalized wave frequency and $\bar{\Omega}_{zo}$ is the nonrelativistic cyclotron frequency due to the applied axial magnetic field. Equations (7) use the following normalization scheme:

(i) the radial coordinate is normalized to r_{wo} ($\bar{r} = r/r_{wo}$), and the axial coordinate is normalized to r_{wo}/x_{mn} ($\bar{z} = z\, x_{mn}/r_{wo}$), where x_{mn} is the nth zero of dJ_m/dx;

(ii) frequencies are normalized to $c/(x_{mn} r_{wo})$ ($\bar{\omega} = \frac{\omega r_{wo}}{c\, x_{mn}}$);

(iii) velocities are normalized to c and momenta are normalized to $m_o c$ ($\bar{v} = v/c$, $u = p/m_o c$);

(iv) electric and magnetic fields are normalized to $\frac{m_o c^2}{|e|} \frac{x_{mn}}{r_{wo}}$ and $\frac{m_o c}{|e|} \frac{x_{mn}}{r_{wo}}$, respectively ($\bar{E} = \frac{|e|}{m_n c^2} \frac{r_{wo}}{x_{mn}} E$, $\bar{B} = \frac{|e|}{m_o c} \frac{r_{wo}}{x_{mn}} B$). Unnormalized quantities are expressed in mks units unless otherwise stated.

In obtaining Equations (7), the radial scale length r_{wo} is assumed to be equal to the waveguide radius and the axial dependence of the waveguide radius has been neglected except in calculating the axial profile function f.

Equations (7) are independent of the wave frequency. Moreover, geometric factors associated with a particular waveguide mode and the position of the electron beam are contained in the factor E_s.

For a circularly polarized mode with azimuthal dependence $e^{-im\theta}$ (and time dependence $e^{i\omega t}$) $\bar{E}_s$ is given by

$$\bar{E}_s = C_{mn}^{(c)} \frac{J_{m-s}}{\bar{r}_w} (\bar{k}_{mn} \bar{R}_o) |\bar{f}_{max}| \bar{e}^{im\Xi_o} \qquad (8)$$

and by

$$\bar{E}_s = C_{mn}^{(c)} (-1)^s \frac{J_{m+s}(\bar{k}_{mn} \bar{R}_o)}{\bar{r}_w} |\bar{f}_{max}| e^{im\Xi_o} \quad (9)$$

for a mode with dependence $e^{+im\theta}$. In Equations (8) and (9) $\bar{r}_w$ is the normalized waveguide radius; $\bar{R}_o$, Ξ_o are the polar coordinates of the electron orbit guiding center orbit and

$$C_{mn}^{(c)} = [[\pi(x_{mn}^2 - m^2)]^{1/2} J_m(x_{mn})]^{-1} \quad (10)$$

The profile function f has dimensions of voltage and is normalized according to $\bar{f} = \frac{|e|}{m_o c^2} f$. The transverse wave number $\bar{k}_{mn} = x_{mn}/\bar{r}_w$.

For a linearly polarized mode with azimuthal dependence cos m θ

$$\bar{E}_s = C_{mn}^{(\ell)} [\frac{J_{m-s}(\bar{k}_{mn} \bar{R}_o)}{\bar{r}_w} e^{-im\Xi_o} + (-1)^s \frac{J_{m+s}}{\bar{r}_w} (\bar{k}_{mn} \bar{R}_o) e^{im\Xi_o}] |f_{max}| \quad (11)$$

where

$$C_{mn}^{(\ell)} = \sqrt{2} [[\pi(x_{mn}^2 - m^2)]^{1/2} J_m (x_{mn})]^{-1} \quad (12)$$

The output power is related to the cavity fields according to

$$P_\omega = \frac{\omega W}{Q} \quad (13)$$

where the stored electromagnetic energy

$$W = \frac{\varepsilon_o}{2} |f_{max}|^2 \int dz |h(z)|^2 \quad (14)$$

and Q is the diffraction Q of the cavity. Substituting Eq. (14) into Eq. (13) and transforming to normalized parameters leads to

$$P_\omega = \frac{1}{2}\frac{c^3}{\mu_0}\left(\frac{m_0}{e}\right)^2 \frac{\bar{\omega}}{\bar{Q}} \left|\bar{f}_{max}\right|^2 \int d\zeta \left|h(z)\right|^2 \qquad (15)$$

where c is the speed of light and $\mu_0 = 4\pi x 10^{-7}$. Eq. (15) shows that the output power is independent of frequency. The electronic efficiency is calculated by integrating Eqs. (7) through the interaction region to obtain the change in electron energy and averaging with respect to the initial momentum phase:

$$\eta = \left[\frac{1}{2\pi}\int_0^{2\pi} d\Lambda_0 \left[\gamma\left(\zeta_F, \Lambda_0\right) - \gamma_0\right]\right] / \left(\gamma - 1\right) \qquad (16)$$

For a linearly polarized mode the efficiency must also be averaged with respect to the guiding center angle Ξ_0. The electron beam power or current are found from the power balance equation:

$$P_b = I_0 V_0 = \frac{P_\omega}{\eta} \qquad (17)$$

The threshold current for oscillation is given by the small signal limit

$$I_{th} = \lim_{E_s \to 0} \frac{P_\omega(E_s)}{V_0 \eta(E_s)} \qquad (18)$$

Calculations of gyrotron efficiency generally assume a circularly polarized rf mode because in this case the interaction efficiency is the same for all beam electrons. When the rf mode is linearly polarized the rf fields have an azimuthal dependence given by sinmθ or cosmθ and consequently the electronic efficiency varies

with azimuthal angle. As shown in Section 3, the result is a reduction in the optimum efficiency averaged over the beam by a factor of approximately 0.7 compared to a circularly polarized mode. Linear mode polarization is nevertheless of particular interest for relativistic gyrotrons as this polarization occurs when axial slots are used to control mode competition.

In these calculations, a value of twice the diffraction limited Q was assumed. The diffraction limited Q is given by

$$Q_D = 4\pi\left(\frac{L}{\lambda}\right)^2 = 4\pi(N_c + 1)^2 \alpha_{\parallel 0}^2 \qquad (19)$$

In gyrotrons the space-charge limited electron beam current places a significant restriction on the achievable output power. An estimate for a thin annular gyro-beam has been derived by Ganguly and Chu[2]. Their result for the space-charge limited current is

$$I_{SCL}(kA) = \frac{8.5\,\gamma_0}{\ell n\,(r_w/r_G)}\left[1 - (1 - \alpha_{\parallel 0}^2)^{1/3}\right]^{3/2} \qquad (20)$$

where r_w is the cavity wall radius and r_G is the e-beam radius.

III. Results of Calculations

This section presents scaling calculations for the relativistic gyrotron. To show the efficiency potential of the relativistic regime and to calibrate the present calculations, Figure 1 compares efficiencies calculated for 70 keV and 1 MeV electron beams with $\alpha = v_\perp/v_\parallel = 1.5$ interacting with a circularly polarized TE mode. One notes that the peak efficiency of 30% at 1 MeV is only slightly less than the peak efficiency of 34% at 70 keV. However, there is an order of magnitude difference in the optimum number of cyclotron orbits: peak efficiency at 1 MeV occurs for N_c = 3-5 whereas peak efficiency at 70 keV occurs for N_c = 15-30. This result is consistent with the gyrotron efficiency scaling relation

$$\eta \sim \frac{1}{N_c(\gamma_o - 1)} \tag{21}$$

derived by Bratman et al[3]. The efficiency results for 70 keV are in good agreement with the results of Chu et al[4] The latter are also shown in Figure 1.

Although the intrinsic efficiency has only a gradual decrease with increase in beam energy other factors limit efficiency at relativistic energies: The efficiency is a sensitive function of the ratio $v_\perp/v_\parallel$ since as shown by Bratman et al[3] $\eta \propto \beta_{\perp o}^2$. Due to lack of experience in the design of high voltage beam formation systems - particularly cold cathode systems - lower values of $v_\perp/v_\parallel$ can be expected, at least initially. As discussed above, the use of a linearly polarized rf mode also reduces efficiency. Figure 2 shows efficiency as a function of N_c for a 600 keV e-beam for α = 1.0 and 1.5 and for linear and circular polarization. For a linearly polarized mode and α = 1.0 -1.5 the peak efficiency is 15% - 22% compared to 21% - 31% for a circularly polarized mode. Similar results for a 1 MeV beam are shown in Figure 3. Effects due to electron beam thermal and self-field effects have not been included. These effects may be significant in a high power, relativistic gyrotron and are under investigation.

Figure 4 shows the optimum electric field vs. N_c both at the electron beam position and at the cavity wall for a linearly polarized mode and a 600 keV beam with $\alpha = 1.5$. The electric field corresponds to the case of a TE_{14} mode with the electron beam placed at the fourth E-field maximum ($r_G/r_w = 0.86$). The curves shown in Figure 4 indicate that the peak cavity field at the wall is reduced an order of magnitude from the field at the beam. Thus peak fields at the beam of $\gtrsim$ 1 MV/cm, which are needed for high power and peak efficiency, can be achieved with low probability of field induced emission from the cavity wall.

Figure 5 shows the electron beam current corresponding to optimum efficiency as a function of N_c for a 600 keV beam. The cavity Q is assumed to be twice the diffraction limited Q and the beam is placed on the fourth E-field maximum. Results are shown for the TE_{14} mode with $\alpha = 1.0$ and 1.5, and for the TE_{15} mode with $\alpha = 1.0$. Linear polarization is assumed in all cases. The estimated space-charge limiting currents for these configurations are: 2.9 kA for the TE_{15} mode with $\alpha = 1.0$, 3.5 kA for the TE_{14} mode with $\alpha = 1.5$ and 7.4 kA for the TE_{14} mode with $\alpha = 1.0$.

Output power scaling at optimum efficiency for a 600 keV beam is shown in Figure 6. The choices for Q and beam position are the same as in Figure 5. The maximum rf power is limited by the dc space charge effect for the TE_{14} mode, $\alpha = 1.5$ and TE_{15} mode, $\alpha = 1.0$ cases. The maximum power for the TE_{14}, $\alpha = 1.0$ case is limited by the available e-beam current of 6 kA corresponding to a Febetron pulser. Figure 7 compares output power scaling for 1 MeV and 0.6 MeV e-beams. The curves correspond to a TE_{14} linearly polarized mode with $\alpha = 1.5$, the beam on the 4^{th} E-field peak, and $Q = 2Q_D$. The 1 MeV curve reaches a peak power of about 1 GW. The dashed curve indicates that higher powers are possible if partial space-charge neutralization proves feasible.

The present analysis has emphasized the high power regime. The interaction region is very short involving only a few cyclotron orbits, and non-linear effects are strong. In this regime the output power is ultimately limited by the condition that the operating e-beam current be greater than the oscillation threshold current. Figure 8 compares the threshold and optimum efficiency currents for a 600 keV beam with $\alpha = 1.5$ placed on the fourth peak of a TE_{14} mode. The optimum efficiency currents are shown for both linear and circular polarization; the former being 10% - 15% larger than the latter. Both polarizations have the same threshold current. Except at short interaction lengths of less than 3 cyclotron orbits, the optimum efficiency current is approximately twice the threshold current. The same behavior is found for a 1 MeV beam.

In the case of short pulse operation it is necessary to consider the output power risetime. The 10% - 90% power risetime is approximately

$$\tau \approx \frac{2Q}{\omega} \left[\frac{I}{I_{thr}} - 1 \right]^{-1} \qquad (22)$$

where I is the beam current and I_{thr} is the threshold current.
This expression does not include the effect of finite e-beam risetime.
Figure 9 shows power risetime scaling vs. N_c for 0.6 MeV and 1 MeV beams with $\alpha = 1.5$, $Q = 2Q_D$. The minimum risetime for a 35 GHz oscillator is shown to be about one nanosecond.

IV. Conclusions

The results of this study indicate that the relativistic gyrotron has potential for achieving high efficiency (15-30%) using relativistic (γ~2-3) electron beams. Optimum efficiency occurs for short interaction lengths characterized by 4-8 cyclotron periods. Such short interaction lengths lead to the possibility of very high peak power generation using multi-kiloampere beams: 100-300 MW for a 600 keV beam and ~ 1 GW with a 1 MeV beam. These power levels apply to the case of single mode operation in a linearly polarized TE_{14} mode.

The optimum interaction efficiency occurs for electric fields ~ 1 MV/cm at the electron beam. Since the gyrotron is based on a fast-wave interaction, such fields at the beam can be achieved without excessive electric fields at the wall. For example, for a 600 keV beam and a TE_{14} mode the peak field at the wall is ~ 100 kV/cm.

The output power rise time has been estimated to be a few nanoseconds for a low Q oscillator at 35 GHz. Thus the gyrotron interaction can be readily investigated using a 20-100 nsec pulseline accelerator.

The electron beam dc space-charge effect appears to be a significant factor limiting gyrotron power. The possibility of space-charge neutralization via a background plasma should be investigated.

V. Acknowledgments

Many helpful and stimulating discussions with Drs. Ganguly, Manheimer, Read, Gold, Dialetis, and Granatstein are gratefully acknowledged. This work was supported by the Defense Nuclear Agency, Lawrence Livermore National Laboratory and the Office of Naval Research.

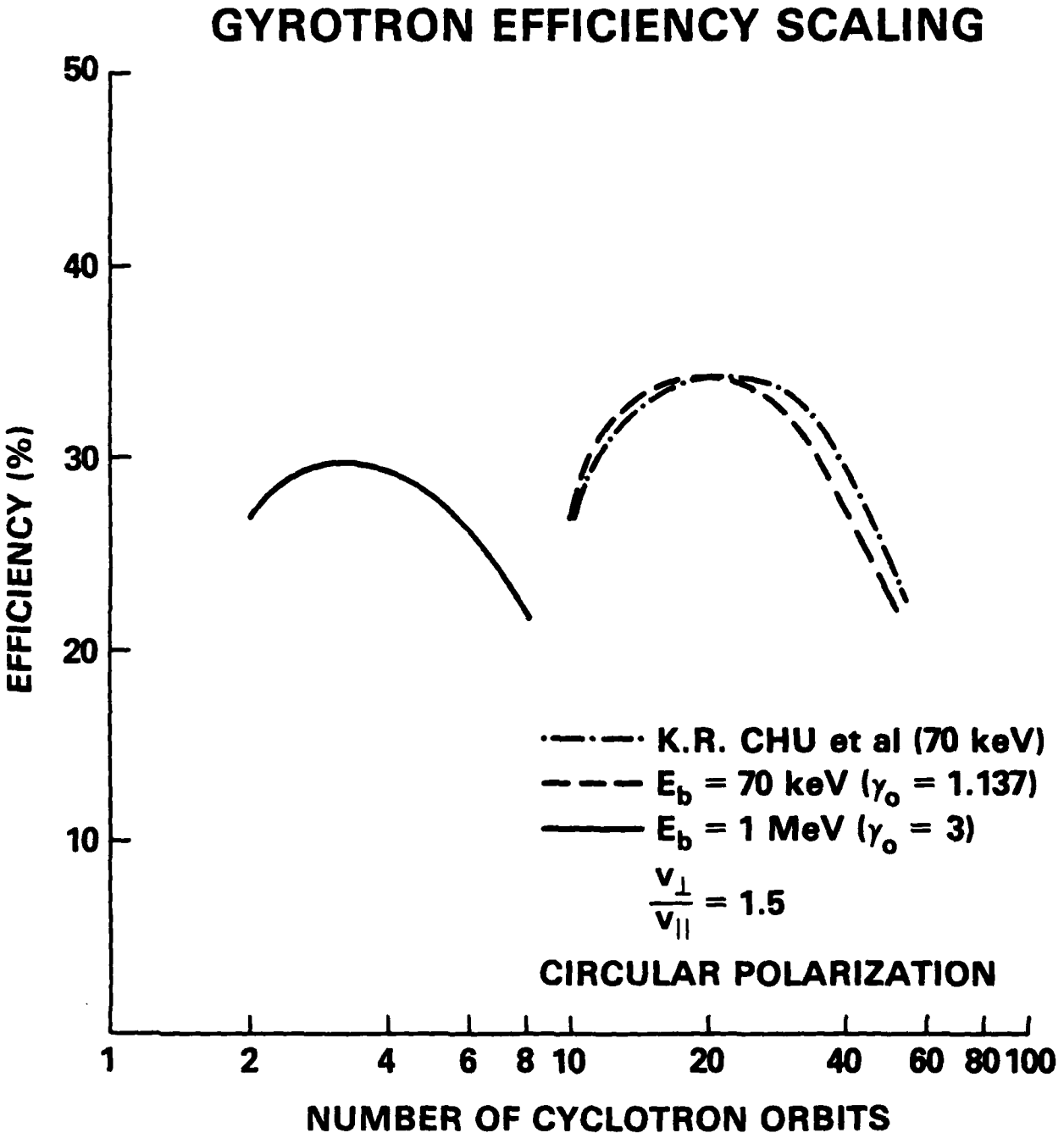

Fig. 1: Optimized Electronic Efficiency as a Function of Interaction Length for a Circularly Polarized TE Mode

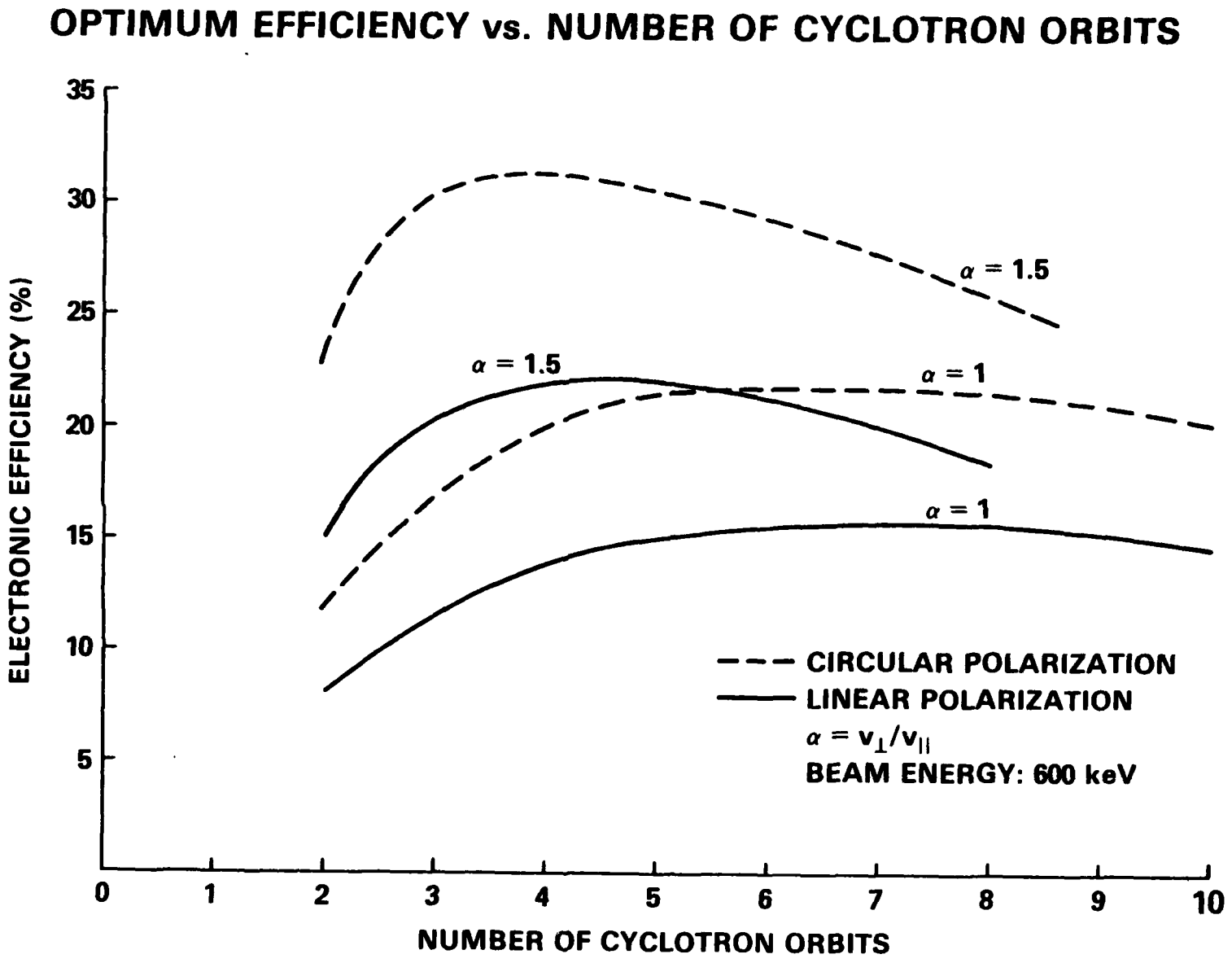

Fig. 2: Optimized Electronic Efficiency for a 600 keV Electron Beam

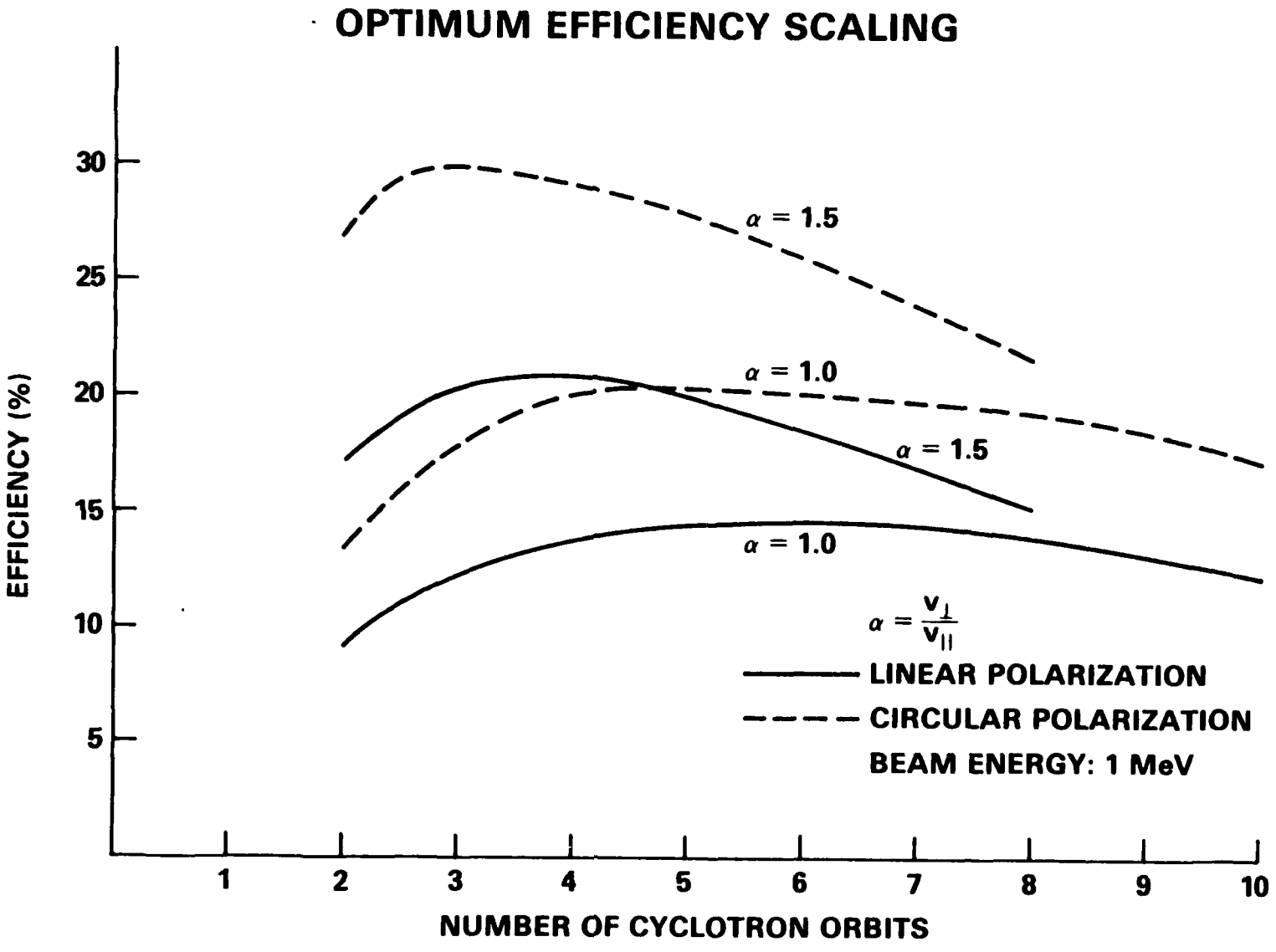

Fig. 3: Optimized Electronic Efficiency for a 1 MeV Electron Beam

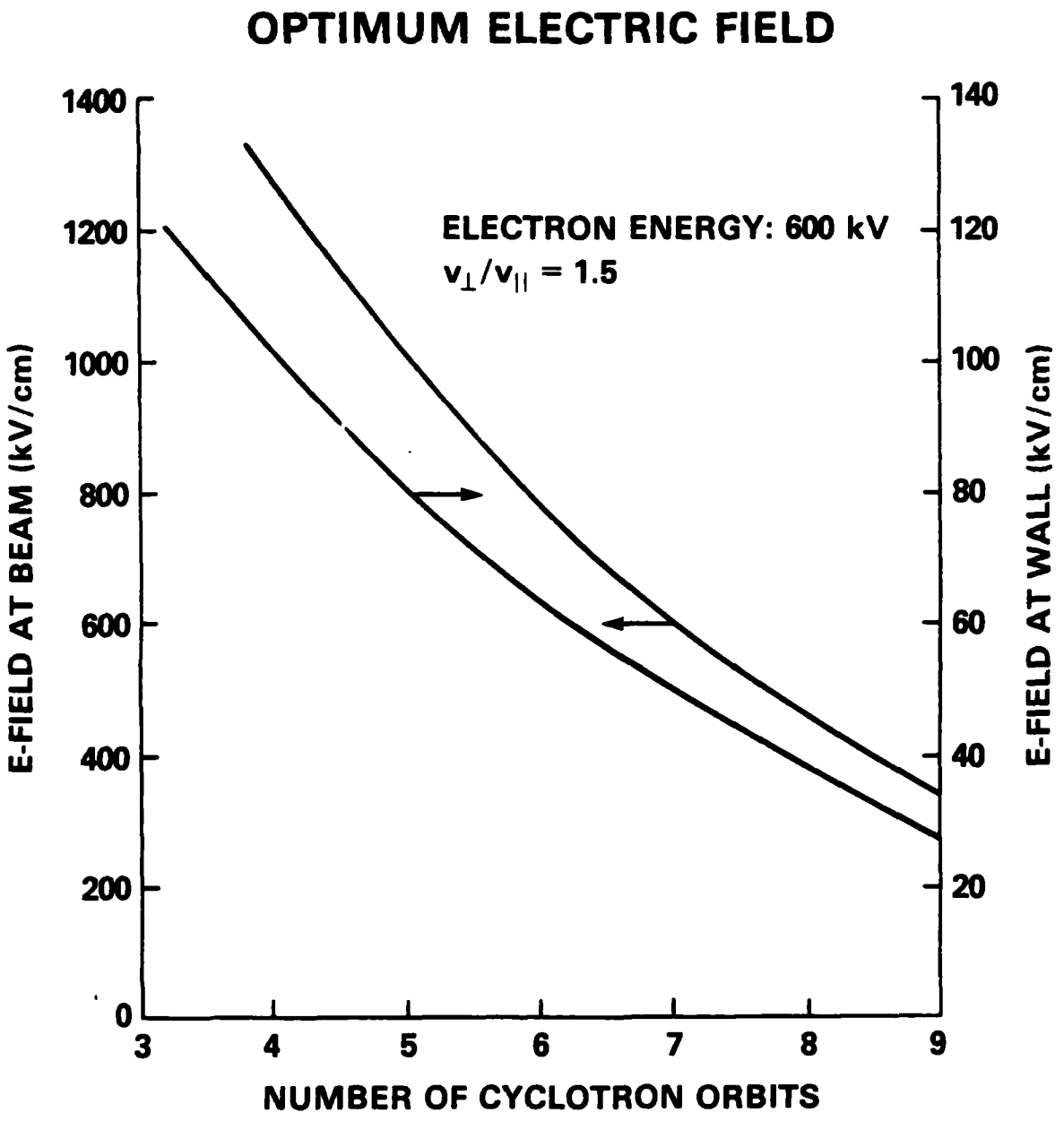

Fig. 4: Optimum Value of the Peak Electric Field at the Electron Beam and at the Cavity Wall for a Linearly Polarized TE_{14} Mode at 35 GHz

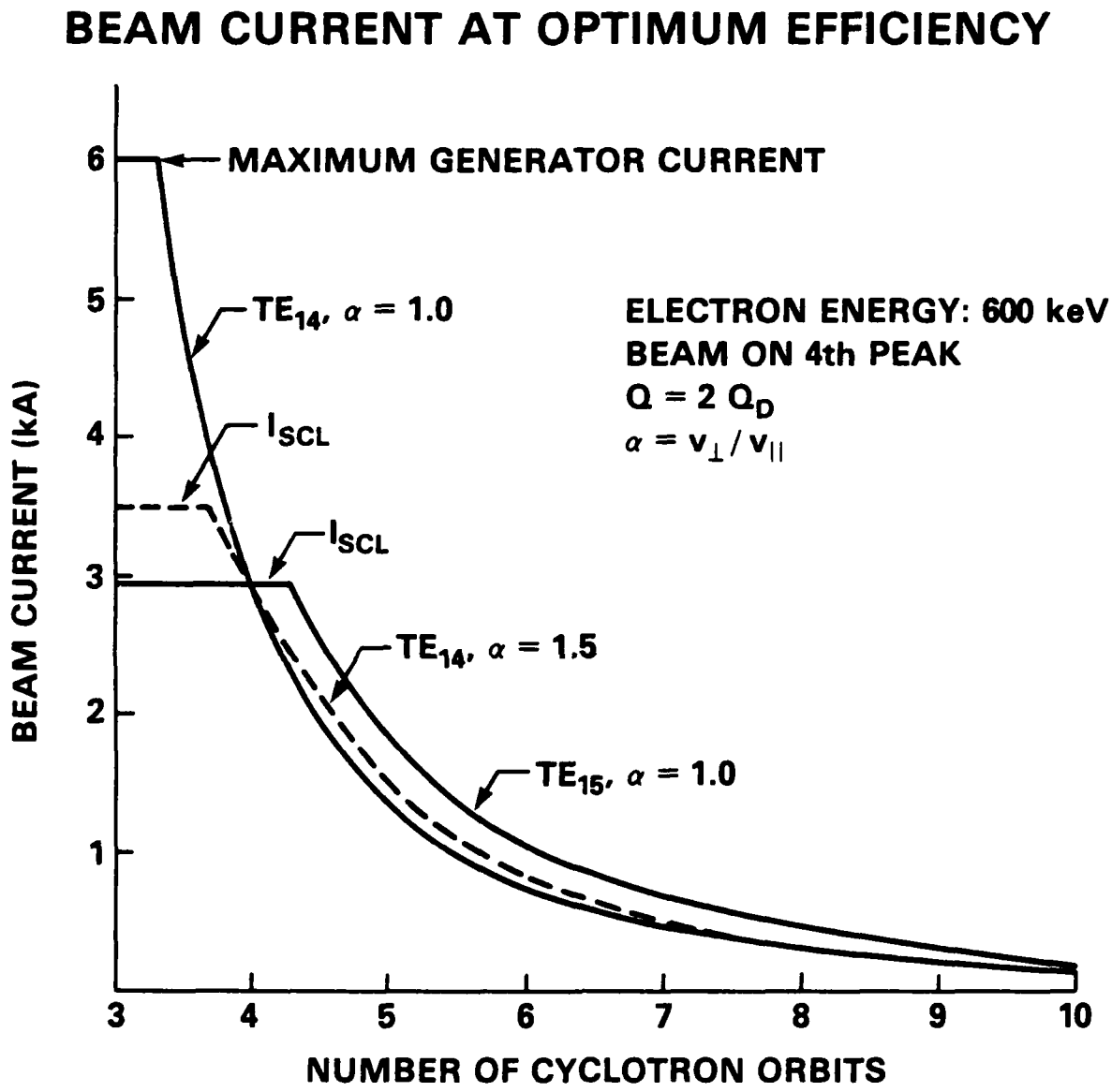

Fig. 5: Electron Beam Current Corresponding to Optimum Efficiency for $Q=2Q_D$ and Linear Polarization. I_{SCL} Denotes the Space-Charge Limited Current. Maximum Generator Current Refers to the NRL 600 kV, 6 kA Febetron Pulser

OUTPUT POWER SCALING

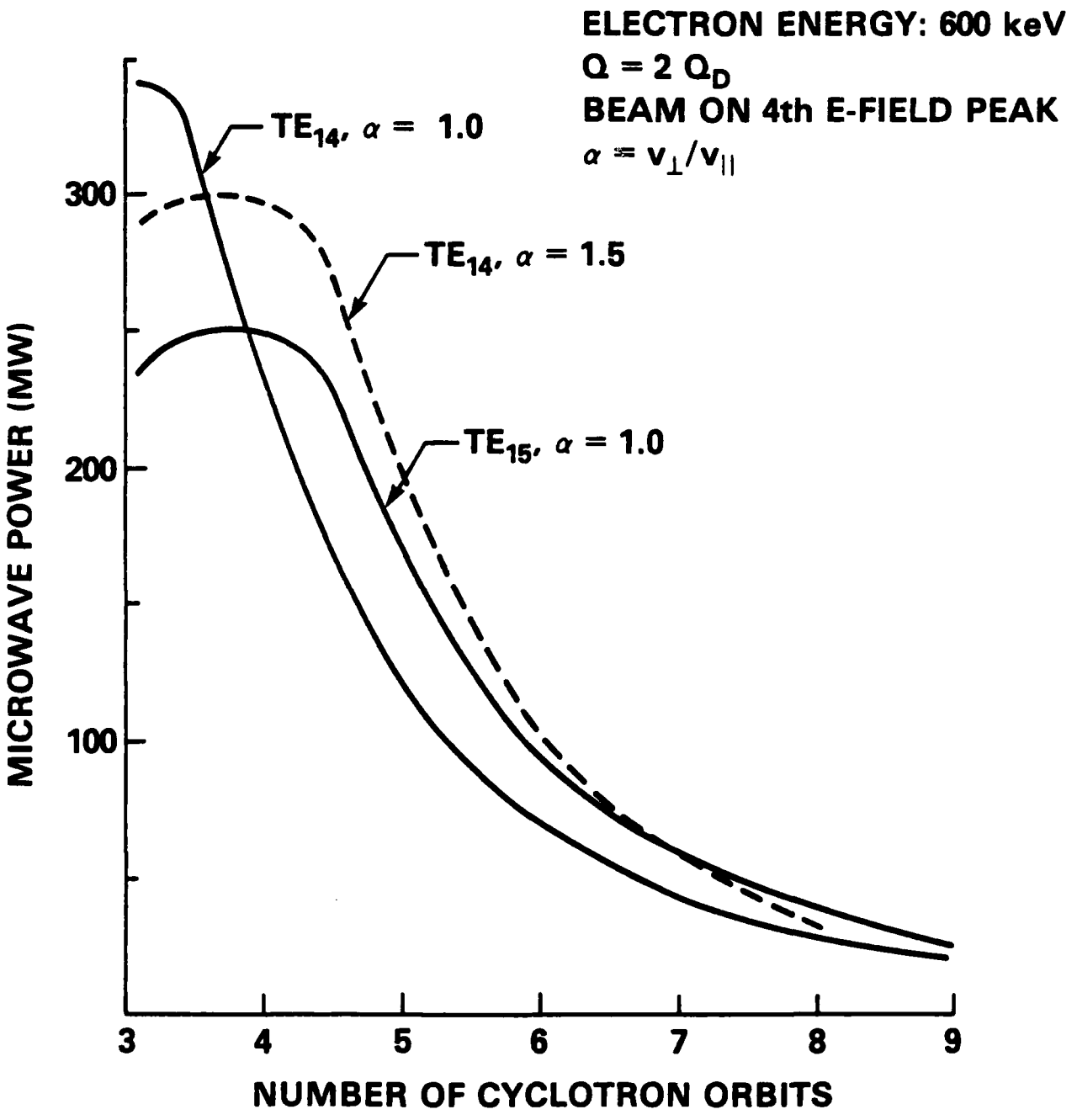

Fig. 6: Output Power Corresponding to Optimum Efficiency Operation for $Q=2Q_D$ and Linear Polarization.

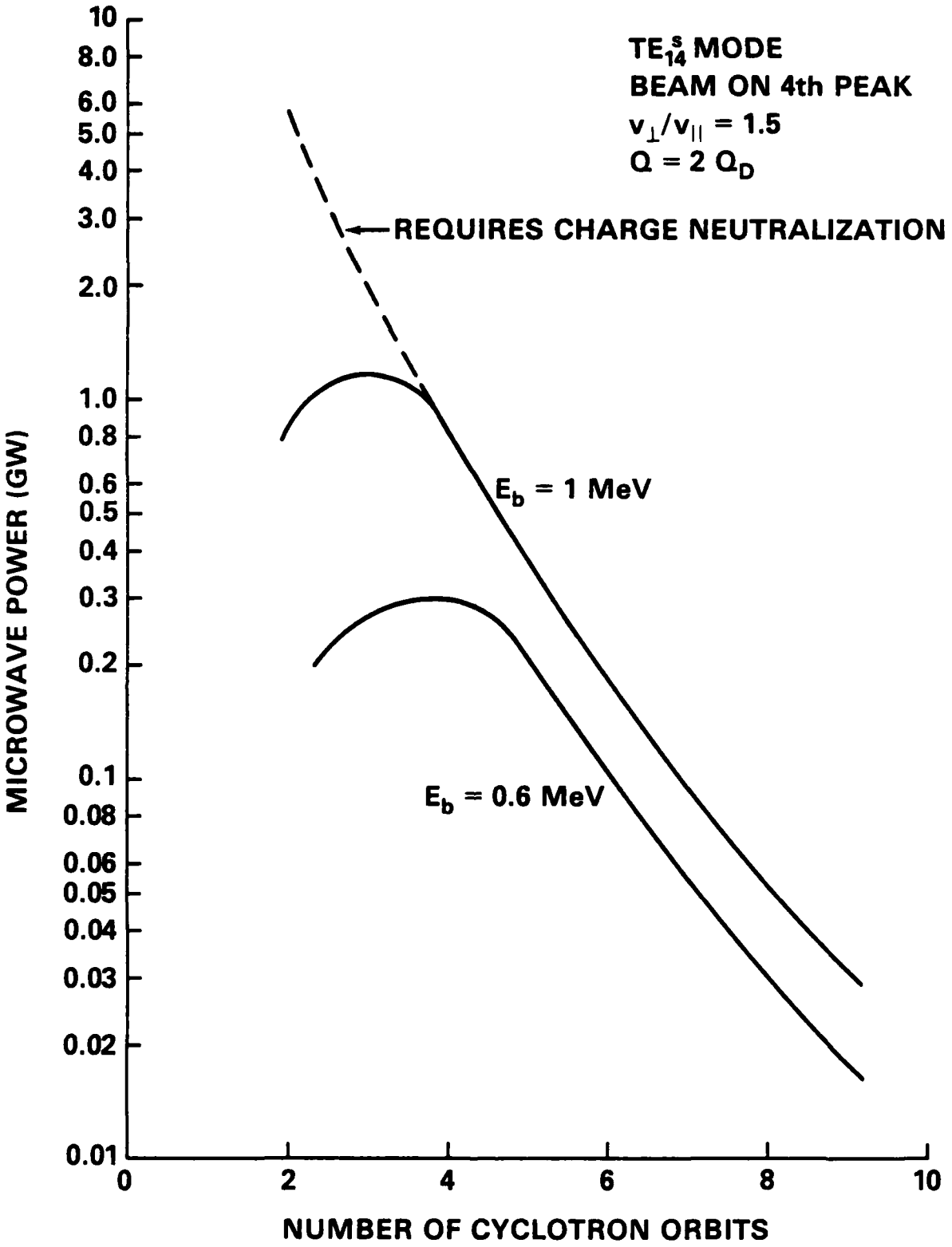

Fig. 7: Output Power for Optimum Efficiency Operation for $Q=2Q_D$ and Linear Polarization. The Dashed Curve Corresponds to Beam Currents Exceeding the Space-Charge Limit and thus not Normally Achievable

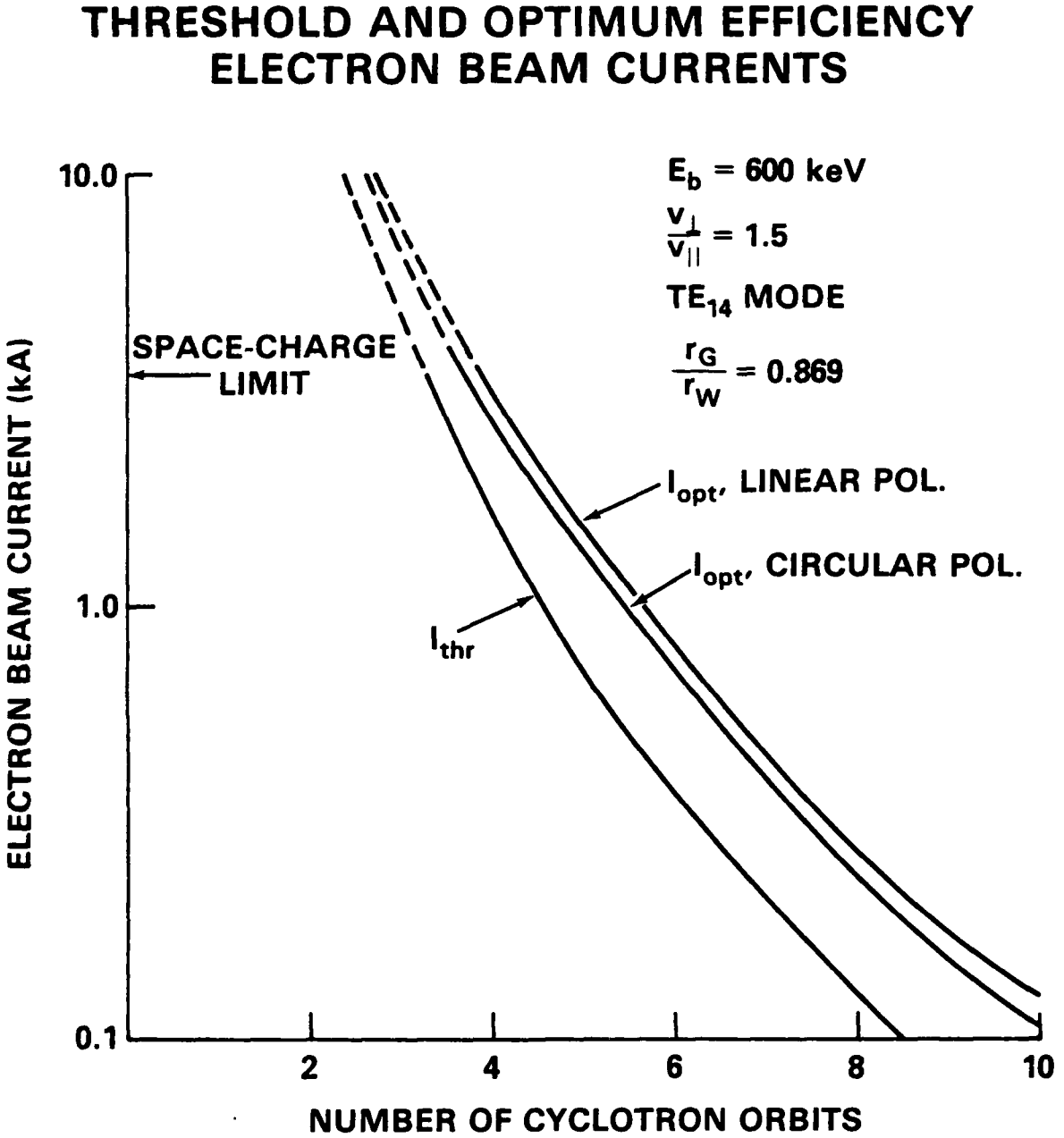

Fig. 8: Comparison of Threshold Beam Current and Current at Optimum Efficiency for Circular and Linear Polarization and $Q=2Q_D$. The Threshold Current is the same for both Polarizations.

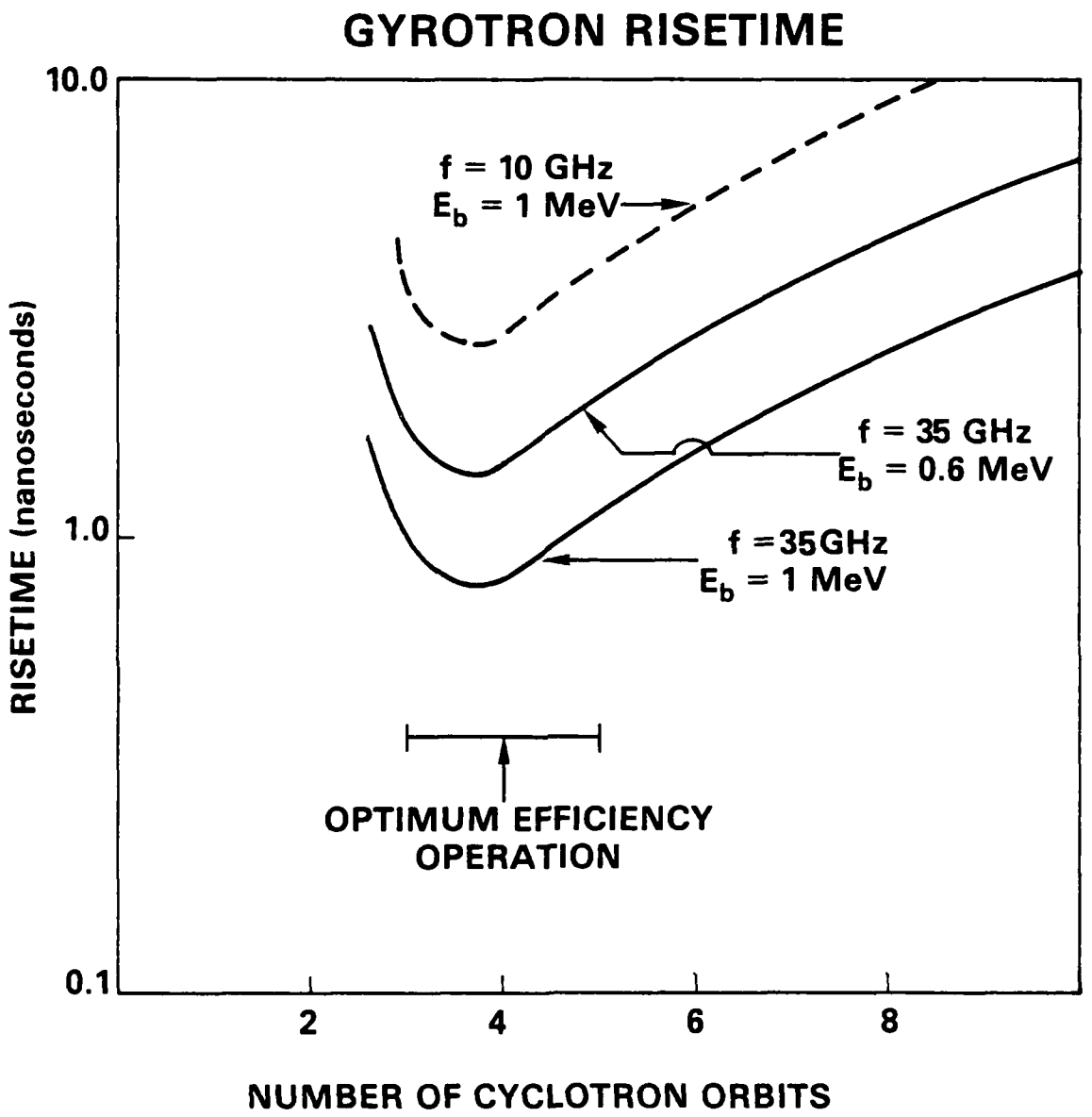

Fig. 9: 10% - 90% Output Power Risetime for a Gyrotron Operating at Optimum Efficiency with $Q=2Q_D$ and $V_\perp/V_\parallel = 1.5$

Appendix

1. Single-Particle Slow-Time-scale Equations of motion

The starting point is the Lorentz force equation

$$\frac{d}{dt}(\gamma\vec{v}) + \eta\,(\vec{v} \times \vec{B}_0) = -\eta\,(\vec{E} + \vec{v} \times \vec{B}) = \vec{a} \tag{1}$$

where $\vec{B}_0$ is an applied static magnetic field which is predominantly axial

$$\vec{B}_0 = B_{oz}\,\hat{z} + B_{or}\,\hat{r}\,, \quad B_{oz} >> B_{or}, \tag{2}$$

$$\eta = \frac{|e|}{m_o} \tag{3}$$

is the charge to rest mass ratio for an electron, and $\vec{E}$, $\vec{B}$ are the electromagnetic fields. It is convenient to introduce the normalized momentum variable

$$\vec{u} = \gamma\vec{v} \tag{4}$$

in terms of which the relativistic factor is given by

$$\gamma = [1 + u^2/c^2]^{1/2} \tag{5}$$

To obtain a slow-time-scale formulation the transverse momentum is expressed in the form:

$$u_x + i\, u_y = i\, u_t \exp\left[i\,(\Omega\,\tau + \phi)\right] \tag{6}$$

where

$$\Omega = \frac{\eta B_o}{\gamma_o} = \frac{\eta B_{oz}(z=o)}{\gamma_o} = \frac{\Omega_{zo}}{\gamma_o} \tag{7}$$

and $\tau = t - t_o$ where t_o is the time the electron enters the interaction region. Using the transformation (6) in Eq. (1) leads to the following equations:

$$\dot{u}_t = \frac{i}{2}\left[(a_x - i a_y)e^{i(\Omega\tau+\phi)} - (a_x + i\, a_y)e^{-i(\Omega\tau+\phi)}\right] + \frac{u_z u_z}{2\gamma}\,\frac{1}{B}\,\frac{\partial B}{\partial z} \tag{8.1}$$

$$\dot{\phi} = \frac{-1}{u_t}\left[(a_x - i a_y)\, e^{i(\Omega\tau+\phi)} + (a_x + i a_y)\, e^{-i(\Omega\tau+\phi)}\right] - \Omega + \frac{\Omega_z}{\gamma} \tag{8.2}$$

$$\dot{u}_z = a_z - \frac{1}{2}\,\frac{1}{B}\,\frac{\partial B}{\partial z}\,\frac{u_t^2}{\gamma} \tag{8.3}$$

Equations 8.1-8.3 account for electron interactions with all rf-field components and allow for a tapered applied magnetic field.

2. Transverse Electromagnetic modes in a waveguide

In the present theory, the electron beam is assumed to interact with a single TE or TM vacuum waveguide mode with time dependence $e^{i\omega t}$. The transverse field components are given by:

$$\vec{E}_t = \mathrm{Re}\left\{f(z)\ \vec{e}\ (x,y,z)\ e^{i\omega t}\right\} \tag{9.1}$$

$$B_t = \mathrm{Re}\left\{g(z)\ \vec{h}\ (x,y,z)\ e^{i\omega t}\right\} \tag{9.2}$$

where $\vec{e}$ and $\vec{h}$ are transverse vector mode functions. These vector functions are related to scalar functicns according to

$$\vec{e} = \hat{z} \times \vec{\nabla}_t \psi \tag{10.1}$$

$$\vec{h} = -\vec{\nabla}_t\ \psi \tag{10.2}$$

for TE modes, and

$$\vec{e} = -\vec{\nabla}_t\ \psi \tag{11.1}$$

$$\vec{h} = -\hat{z} \times \vec{\nabla}_t\ \psi \tag{11.2}$$

for TM modes, The scalar functions satisfy the equation

$$(\nabla_t^2 + k_\perp^2)\ \psi = 0 \tag{12}$$

and the boundary condition

$$\frac{\partial \psi}{\partial n} = 0 \tag{13.1}$$

on the waveguide boundary for TE modes, or

$$\psi = 0 \tag{13.2}$$

at the waveguide boundary for TM modes. In Eq. (13.1) $\partial/\partial n$ indicates the normal derivitive. When integrated over the waveguide cross section the vector functions satisfy the normalization and orthogonality conditions

$$\int_{S(z)} dxdy \; \vec{v}_i \vec{v}_j = \delta_{ij} \tag{14}$$

($\delta_{ij} = 0$ if $i \neq j$, $\delta_{ij} = 1$ if $i = j$) where $\vec{v}_i$ denotes either $\vec{e}_i$ or $\vec{h}_i$ and $S(z)$ denotes the z-dependent waveguide cross section. The axial field components are given by

$$B_z = \text{Re}\left\{-i \frac{k_\perp^2}{w} f(z) \; \psi \; (x,y) \; e^{i\omega t}\right\} \tag{15}$$

for a TE mode, and by

$$E_z = \text{Re}\left\{-i \frac{c^2}{\omega} k_\perp^2 \; g(z) \; \psi \; (x,y) e^{i\omega t}\right\} \tag{16}$$

for a TM mode. The axial profile functions f(z) and g(z) are related according to

$$g(z) = \frac{i}{\omega} \frac{df(z)}{dz} \tag{17}$$

for a TE mode, and

$$f(z) = i \frac{c^2}{\omega} \frac{dg(z)}{dz} \tag{18}$$

for a TM mode. Equations (15-18) are obtained by substitution into the Maxwell curl equation

$$\vec{\nabla} \times \vec{E} = - \frac{\partial \vec{B}}{\partial t} \tag{19}$$

3. Equations of motion for an electron interacting with a waveguide mode

Substituting Equation (9) - (16) into (8) leads to

$$\dot{u}_t = \mathrm{Re}\left\{-\eta\ (f - v_z g)\ (L_+ \psi e^{-i(\Omega\tau+\phi)} + L_- \psi\ e^{i(\Omega\tau+\phi)})\ e^{i\omega t}\right\}$$

$$+ \frac{u_z u_t}{2\gamma}\ \frac{1}{B_z}\ \frac{\partial R_z}{\partial z} \tag{20.1}$$

$$\dot{\phi} = \frac{1}{u_t}\ \mathrm{Re}\left\{\frac{in}{2}\left[(f - v_z g)\ (L_+ \psi e^{-i(\Omega\tau+\phi)} - L_- \psi e^{i(\Omega\tau+\phi)}\right)\right.$$

$$\left. -2\ \frac{v_t k_t^2}{\omega} f\psi\ \right] e^{i\omega t}\Big\} - \Omega + \frac{\Omega_z}{\gamma} \tag{20.2}$$

$$\dot{u}_z = \mathrm{Re}\left\{-\frac{n v_t}{2}\ g\ (L_+ \psi\ e^{-i(\Omega\tau+\phi)} + L_- \psi\ e^{i(\Omega\tau+\phi)}\ e^{i\omega t}\right\}$$

$$- \frac{u_t^2}{2\gamma}\ \frac{1}{B_z}\ \frac{\partial R_z}{\partial z} \tag{20.3}$$

for TE modes, and

$$\dot{u}_t = \mathrm{Re}\{-in(f - v_z g)\ (L_+ \psi e^{-i(\Omega\tau+\phi)} - L_- \psi e^{i(\Omega\tau+\phi)}) e^{i\omega t}\}$$

$$+ \frac{u_z u_t}{2\gamma_z}\ \frac{1}{B_z}\ \frac{\partial R_z}{\partial z} \tag{21.1}$$

$$\dot{\phi} = \frac{1}{u_t} \mathrm{Re} \left\{ -\frac{n}{2} (f - v_z g) \left(L_+ \psi e^{-i(\Omega\tau+\phi)} + L_- \psi \, e^{i(\Omega\tau+\psi)} \right) e^{i\omega t} \right\}_{-\Omega} + \frac{\Omega_z}{\gamma} \quad (21.1)$$

$$\dot{u}_z = \mathrm{Re} \left\{ -\frac{in}{2} g \left[v_t \left(L_+ \psi e^{-i(\Omega\tau+\phi)} - L_- \psi e^{i(\Omega\tau+\phi)} \right) \right. \right.$$

$$\left. \left. + 2 \frac{c^2 k_t^2}{\omega} \psi \right] e^{i\omega t} \right\} - \frac{1}{2B_z} \frac{\partial B_z}{\partial z} \frac{u_t^2}{\gamma} \quad (21.3)$$

for TM modes, where L_+ and L_- are defined by:

$$L_+ \psi \equiv e^{i\theta} \left(\frac{\partial}{\partial r} + \frac{i}{r} \frac{\partial}{\partial \theta} \right) \psi, \quad (22.1)$$

$$L_- \psi \equiv e^{-i\theta} \left(\frac{\partial}{\partial r} - \frac{i}{r} \frac{\partial}{\partial \theta} \right) \psi. \quad (22.2)$$

3.1 Circular waveguide mode.

For a circular waveguide, the projection of an electron orbit on the cross sectional plane of the resonator forms an annulus with average radius equal to the electron orbit guiding center radius R_0, and with thickness equal to twice the Larmor radius

$$r_L \equiv u_t / \Omega_z \quad (23)$$

The case of an axis encircling beam ($R_0=0$) is a special case of the analysis.

The scalar function for a circular waveguide mode with circular polarization is

$$\psi_{mn} = C_{mn} J_m (k_{mn} r) e^{\pm im\theta} \quad (24)$$

where for a TE mode:

$$k_{mn} = \frac{x_{mn}}{r_w} , \tag{25}$$

$$C_{mn} = [[\pi (x_{mn}^2 - m^2)]^{1/2} J_m(x_{mn})]^{-1} , \tag{26}$$

x_{mn} is the n^{th} zero of $J_m'(x)$ (prime denotes differentiation), J_m is a Bessel function, and r_w is the waveguide wall radius. For a TM mode:

$$k_{mn} = \frac{z_{mn}}{r_\omega} , \tag{27}$$

$$C_{mn} = [\sqrt{\pi}\, z_{mn}\, J_m (z_{mn})]^{-1} , \tag{28}$$

and z_{mn} is the n^{th} zero of $J_m(z)$. For definitness consider the mode with polarization $e^{i(\omega t - m\theta)}$. Substitution of Eq. (24) into (22.1) and (22.2) gives

$$L_+\psi = C_{mn}\, k_{mn}\, J_{m-1}(k_{mn} r) e^{-i(m-1)\theta} \tag{29.1}$$

$$L_-\psi = C_{mn}\, k_{mn}\, J_{m+1}(k_{mn} r)\, e^{-i(m+1)\theta} \tag{29.2}$$

For the case of non-zero guiding center radius, the addition theorem[5] is used to express Bessel functions of the radial coordinate in terms of Bessel functions with guiding center and Larmor radius arguments; i.e.,

$$J_m(kr)\, e^{\pm im\theta} = \sum_k J_{m+k}(kR_o)\, J_k(kr_L) e^{\pm ik[\pi - (\Omega\tau + \phi) \pm (k+m)\Xi_o]} \tag{30}$$

where Ξ_o is guiding center position angle.

Substitution of Equations (24), (29), and (30) into (20) or (21), and considering

the interaction with the sth harmonic of the applied magnetic field leads to the following slow time-scale equations of motion: For a TE mode:

$$\dot{u}_t = \mathrm{Re}\left\{-\eta\,(f-v_z g)\,C_{mn} J_{m-s}(k_{mn}R_o)\,\frac{\partial J_s(k_{mn}r_L)}{\partial r_L}\right.$$

$$\left. e^{\,i[(\omega-s\Omega)\tau + \omega t_o - s\phi - (m-s)\Xi_o]}\right\} + \frac{u_z u_t}{2\gamma}\,\frac{1}{B_z}\,\frac{\partial B_z}{\partial z} \qquad (31.1)$$

$$\dot{\phi} = \frac{1}{u_t}\,\mathrm{Re}\left\{\, i\eta\left[(f-v_z g) - \frac{k_{mn}^2\,u_t}{\gamma s\omega\,\Omega_z} f\right] C_{mn}\, J_{m-s}(k_{mn}R_o)\,\frac{s}{r_L}\,J_s(k_{mn}r_L)\right.$$

$$\left. e^{i[(\omega-s\Omega)\,\tau + \omega t_o - s\phi - (m-s)\,\Xi_o]}\right\} - \Omega + \frac{\Omega_z}{\gamma} \qquad (31.2)$$

$$\dot{u}_z = \mathrm{Re}\left\{-\eta g\,\frac{u_t}{\gamma}\,C_{mn}\,J_{m-s}(k_{mn}R_o)\,\frac{\partial J_s}{\partial r_L}(k_{mn}r_L)\right.$$

$$\left. e^{i[(\omega - s\Omega\tau + \omega t_o - s\phi - (m-s)\,\Xi o]}\right\} \quad \frac{1}{2}\,\frac{u_t^2}{\gamma}\,\frac{1}{B_z}\,\frac{\partial B_z}{\partial z}\,. \qquad (31.3)$$

and for a TM mode:

$$\dot{u}_t = \mathrm{Re}\left\{-i\eta\,(f-v_z g)\,C_{mn}\,J_{m-s}(k_{mn}R_o)\,\frac{s}{r_L}\,J_s(k_{mn}r_L)\right.$$

$$\left. e^{\,i[(\omega-s\Omega)\tau + \omega t_o - s\phi - (m-s)\,\Xi o]}\right\} + \frac{u_z u_z}{2\gamma}\,\frac{1}{B_z}\,\frac{\partial B_z}{\partial z} \qquad (32.1)$$

$$\dot{\phi} = \frac{1}{u_t}\,\mathrm{Re}\left\{-\eta(f-v_z g)\,J_{m-s}(k_{mn}R_o)\,\frac{\partial J_s}{\partial r_L}(k_{mn}r_L)\right.$$

$$\left. e^{i[(\omega-s\Omega)\tau + \omega t_o - s\phi - (m-s)\,\Xi_o]}\right\} - \Omega + \frac{\Omega z}{\gamma} \qquad (32.2)$$

$$\dot{u}_z = \mathrm{Re}\left\{-\eta g\left(\frac{u_t}{\gamma} - \frac{c^2 k_{mn} r_L}{s\omega}\right) C_{mn}\,J_{m-s}(k_{mn}R_o)\,\frac{s}{r_L}\,J_s(k_{mn}r_L)\right.$$

$$\left. e^{i[(\omega-s\Omega)\tau + \omega t_o - s\phi - (m-s)\Xi]_o}\right\} \frac{u_t^2}{2\gamma}\,\frac{1}{B}\,\frac{\partial B_z}{\partial z} \qquad (32.3)$$

In Eqs. (7) in Section 2, above the phase angle ϕ is replaced by

$$\Lambda \equiv (\omega - s\Omega)\tau + \omega\tau_o - s\phi - (m-s)\Xi_o . \tag{33}$$

REFERENCES

1. A.W. Fliflet, M.E. Read, K.R. Chu, and R. Seeley, "A Self-Consistent Field Theory for Gyrotron Oscillators: Application to a Low Q Gyromonotron", International Journal of Electronics 53, 505 (1982).

2. A.K. Ganguly and K.R. Chu, "Limiting Current in Gyrotron", International Journal of Electronics 55, 103 (1984).

3. V.L. Bratman, N.S. Ginzburg, G.S. Nusinovich, M.I. Petelin and P.S. Strelkov, "Relativistic Gyrotrons and Cyclotron Autoresonance Masers", International Journal of Electronics 51, 541 (1981).

4. K.R. Chu, M.E. Read, and A.K. Ganguly, "Methods of Efficiency Enhancement and Scaling for the Gyrotron Oscillator", IEEE Transaction on Microwave Theory and Techniques, MTT-28; 316 (1980).

5. M. Abramowitz and I.A. Stegun, "Handbook of Mathematical Functions" (New York: Dover Publications 1970), p. 355.

DISTRIBUTION LIST

Air Force Avionics Laboratory
AFWAL/AADM-1
Wright/Patterson AFB, Ohio 45433
Attn: Walter Friez — 1 copy

Air Force Office of
Scientific Research
Bolling AFB
Washington, D.C. 20332
Attn: H. Schlossberg — 1 copy

Air Force Weapons Lab
Kirkland AFB
Albuquerque, New Mexico 87117
Attn: J. Generosa — 1 copy
C. Clark — 1 copy

Columbia University
520 West 120th Street
Department of Electrical Engineering
New York, N.Y. 10027
Attn: Dr. S.P. Schlesinger — 1 copy

Columbia University
520 West 120th Street
Department of Applied Physics
and Nuclear Engineering
New York, New York 10027
Attn: T.C. Marshall — 1 copy

Cornell University
School of Applied and Engineering Physics
Ithica, New York 14853
Attn: Prof. Hans H. Fleischmann — 1 copy
John Nation — 1 copy

Dartmouth College
18 Wilder, Box 6127
Hanover, New Hampshire 03755
Attn: Dr. John E. Walsh — 1 copy

Department of Energy
Washington, D.C. 20545
Attn: C. Finfgeld/ER-542, GTN — 1 copy
T.V. George/ER-531, GTN — 1 copy
D. Crandall/ER-55, GTN — 1 copy

Defense Advanced Research Project Agency/DEO
1400 Wilson Blvd.
Arlington, Virginia 22209
Attn: Dr. S. Shey — 1 copy

Defense Communications Agency
Washington, D.C. 20305
Attn: Dr. Pravin C. Jain
Assistant for Communications
Technology — 1 copy

Defense Nuclear Agency
Washington, D.C. 20305
Attn: Mr. J. Farber — 1 copy
Maj. J. Benson — 1 copy
Capt. D. Stone — 1 copy
Mr. Lloyd Stossell — 1 copy

Defense Technical Information Center
Cameron Station
5010 Duke Street
Alexandria, Virginia 22314 — 2 copies

Georgia Tech. EES-EOD
Baker Building
Atlanta, Georgia 30332
Attn: Dr. James J. Gallagher — 1 copy

Hanscomb Air Force Base
Stop 21, Massachusetts 01731
Attn: Lt. Rich Nielson/ESD/INK — 1 copy

Hughes Aircraft Co.
Electron Dynamics Division
3100 West Lomita Boulevard
Torrance, California 90509
Attn: J. Christiansen — 1 copy
J.J. Tancredi — 1 copy

KMS Fusion, Inc.
3941 Research Park Dr.
P.O. Box 1567
Ann Arbor, Michigan 48106
Attn: S.B. Segall — 1 copy

Lawrence Livermore National Laboratory
P.O. Box 808
Livermore, California 94550
Attn: Dr. D. Prosnitz — 1 copy
Dr. T.J. Orzechowski — 1 copy
Dr. J. Chase — 1 copy

Los Alamos Scientific Laboratory
P.O. Box 1663, AT5-827
Los Alamos, New Mexico 87545
Attn: Dr. J.C. Goldstein — 1 copy
Dr. T.J.T. Kwan — 1 copy
Dr. L. Thode — 1 copy
Dr. C. Brau — 1 copy

Massachusetts Institute of Technology
Department of Physics
Cambridge, Massachusetts 02139

Attn: Dr. G. Bekefi/36-213	1 copy
Dr. M. Porkolab/NW 36-213	1 copy
Dr. R. Davidson/NW 16-206	1 copy
Dr. A. Bers/NW 38-260	1 copy

Massachusetts Institute of Tech.
167 Albany St., N.W. 16-200
Cambridge, Massachusetts 02139

Attn: Dr. R. Temkin/NW 14-4107	1 copy

Mathematical Sciences Northwest, Inc.
Bellevue, Washington 90004

Attn: Dr. J.M. Slater	1 copy

Mission Research Corp.
1720 Randolph Road, S.E.
Albuquerque, New Mexico 87106

Attn: Dr. Ken Busby	1 copy
Mr. Brendan B. Godfrey	1 copy

Naval Electronic Systems Command
Washington, D.C. 20363

Attn: E. Warden	
Code PDE 106-3113	1 copy

Naval Research Laboratory

Addressee: Attn: Name/Code	
Code 1001 - T. Coffey	1 copy
Code 2628 - TID Distribution	22 copies
Code 4000 - W. Ellis	1 copy
Code 4700 - S. Ossakow	26 copies
Code 4700.1 - A.W. Ali	1 copy
Code 4704 - C. Kapetanakos	1 copy
Code 4740 - Branch Office	25 copies
Code 4740 - W. Black	1 copy
Code 4740 - J. Condon	1 copy
Code 4740 - A. Fliflet	1 copy
Code 4740 - S. Gold	1 copy
Code 4740 - A. Kinkead	1 copy
Code 4740 - W.M. Manheimer	1 copy
Code 4740 - M.E. Read	1 copy
Code 4740 - M. Rhinewine	1 copy
Code 4770 - G. Cooperstein	1 copy
Code 4790 - B. Hui	1 copy
Code 4790 - C.M. Hui	1 copy
Code 4790 - Y.Y. Lau	1 copy
Code 4790 - P. Sprangle	1 copy
Code 5700 - L.A. Cosby	1 copy
Code 6840 - S.Y. Ahn	1 copy
Code 6840 - A. Ganguly	1 copy
Code 6840 - R.K. Parker	1 copy

Code 6840 - N.R. Vanderplaats 1 copy
Code 6850 - L.R. Whicker 1 copy
Code 6875 - R. Wagner 1 copy

Naval Sea Systems Command
Department of the Navy
Washington, D.C. 20362
Attn: Commander George Bates
PMS 405-300 1 copy

Northrop Corporation
Defense Systems Division
600 Hicks Rd.
Rolling Meadows, Illinois 60008
Attn: Dr. Gunter Dohler 1 copy

Oak Ridge National Laboratory
P.O. Box Y
Mail Stop 3
Building 9201-2
Oak Ridge, Tennessee 37830
Attn: Dr. A. England 1 copy
M. Loring 1 copy

Office of Naval Research
800 N. Quincy Street
Arlington, Va. 22217
Attn: Dr. C. Roberson 1 copy
Dr. W. Condell 1 copy
Dr. T. Berlincourt 1 copy

Office of Naval Research
1030 E. Green Street
Pasadena, CA 91106
Attn: Dr. R. Behringer 1 copy

Optical Sciences Center
University of Arizona
Tucson, Arizona 85721
Attn: Dr. Willis E. Lamb, Jr. 1 copy

Pacific Missile Test Center
Code 0141-5
Point Muga, California 93042
Attn: Will E. Chandler 1 copy

Physical Dynamics, Inc.
P.O. Box 10367
Oakland, California 94610
Attn: A. Thomson 1 copy

Physics International
2700 Merced Street
San Leandro, California 94577
Attn: Dr. J. Benford — 1 copy

Princeton Plasma
Plasma Physics Laboratory
James Forrestal Campus
P.O. Box 451
Princeton, New Jersey 08544
Attn: Dr. H. Hsuan — 2 copies

Quantum Institute
University of California
Santa Barbara, California 93106
Attn: Dr. L. Elias — 1 copy

Raytheon Company
Microwave Power Tube Division
Foundry Avenue
Waltham, Massachusetts 02154
Attn: N. Dionne — 1 copy

Sandia National Laboratories
ORG. 1231, P.O. Box 5800
Albuquerque, New Mexico 87185
Attn: Dr. Thomas P. Wright — 1 copy
Mr. J.E. Powell — 1 copy
Dr. J. Hoffman — 1 copy
Dr. W.P. Ballard — 1 copy

Science Applications, Inc.
1710 Goodridge Dr.
McLean, Virginia 22102
Attn: Adam Drobot — 1 copy

Stanford University
High Energy Physics Laboratory
Stanford, California 94305
Attn: Dr. T.I. Smith — 1 copy

TRW, Inc.
Space and Technology Group
Suite 2600
1000 Wilson Boulevard
Arlington, VA 22209
Attn: Dr. Neil C. Schoen — 1 copy

TRW, Inc.
Redondo Beach, California 90278
Attn: Dr. H. Boehmer — 1 copy

University of California
Physics Department
Irvine, California 92717
Attn: Dr. G. Benford — 1 copy
Dr. N. Rostoker — 1 copy

University of California
Department of Physics
Los Angeles, CA 90024
Attn: Dr. A.T. Lin — 1 copy
Dr. N. Luhmann — 1 copy
Dr. D. McDermott — 1 copy

University of Maryland
Department of Electrical Engineering
College Park, Maryland 20742
Attn: Dr. V. L. Granatstein — 1 copy

University of Maryland
Laboratory for Plasma and Fusion
Energy Studies
College Park, Maryland 20742
Attn: Dr. Jhan Varyan Hellman — 1 copy
Dr. John McAdoo — 1 copy

University of Tennessee
Dept. of Electrical Engr.
Knoxville, Tennessee 37916
Attn: Dr. I. Alexeff — 1 copy

University of New Mexico
Department of Physics and Astronomy
800 Yale Blvd, N.E.
Albuquerque, New Mexico 87131
Attn: Dr. Gerald T. Moore — 1 copy

University of Utah
Deparment of Electrical Engineering
3053 Merrill Engineering Bldg.
Salt Lake City, Utah 84112
Attn: Dr. Larry Barnett — 1 copy
Dr. J. Mark Baird — 1 copy

Varian Associates
611 Hansen Way
Palo Alto, California 94303
Attn: Dr. H. Jory — 1 copy
Dr. David Stone — 1 copy
Dr. Kevin Felch — 1 copy

Westinghouse Electric Corporation
1310 Beulah Road
Pittsburgh, Pennsylvania 15235
Attn: Dr. Anthony Lee — 1 copy

Yale University
Applied Physics
Madison Lab
P.O. Box 2159
Yale Station
New Haven, Connecticut 06520
Attn: Dr. J. Hirshfield — 1 copy
Dr. N. Ebrahim — 1 copy
Dr. I. Bernstein — 1 copy

Director of Research
U.S. Naval Academy
Annapolis, MD 21402 — 2 copies

END

FILMED

9-85

DTIC